Chemistry–A European Journal
Research Article
doi.org/10.1002/chem.202104591
Chemistry Europe
European Chemical Societies Publishing
www.chemeurj.org

π-Conjugated Copper Phthalocyanine Nanoparticles as Highly Sensitive Sensor for Colorimetric Detection of Biomarkers

Fan Chen,[a] Huang Zhu,[a] Ning Lv,[a] Qian Li,[a] Tian Ma,[b] Liyun Wang,[b] Mi Zhou,[c] Sujiao Cao,*[b] Xianglin Luo,*[a] and Chong Cheng[a]

Abstract: Though numerous nanomaterials with enzyme-like activities have been utilized as probes and sensors for detecting biological molecules, it is still challenging to construct highly sensitive detectors for biomarkers using polymeric materials. Benefiting from the π-d delocalization effect of electrons, excellent metal-chelating property, high electron transferability, and good chemical stability of π-conjugated phthalocyanine, the design of the copper phthalocyanine-based conjugated polymer nanoparticles (Cu-PcCP NPs) as a colorimetric sensor for a variety of biomarkers is reported. The Cu-PcCP NPs are synthesized through a simple microwave-assisted polymerization, and their chemical structures are thoroughly characterized. The colorimetric results of Cu-PcCP NPs demonstrate excellent peroxidase-like detecting activity and also great substrate selectivity than most of the reported Cu-based nanomaterials. The Cu-PcCP NPs can achieve a detection limit of 4.88 μM for the H_2O_2, 4.27 μM for the L-cysteine, and 21.10 μM for the glucose via a cascade catalytic system, which shows comparable detecting sensitivity as that of many earlier reported enzyme-like nanomaterials. Moreover, Cu-PcCP NPs present remarkable resistance to harsh conditions, including high temperature, low pH, and excessive salts. These highly specific π-conjugated copper-phthalocyanine nanoparticles not only overcome the current limitation of polymeric material-based sensors but also provide a new direction for designing next-generation enzyme-like nanomaterial-based colorimetric biosensors.

Introduction

Biosensor-mediated detection of biomolecules has become an increasingly important issue in a variety of areas, especially in disease diagnoses and therapies.[1] Abundant natural enzymes, possessing both high substrate specificity and catalytic efficiency for various biological reactions, have been proven as excellent biosensors for detecting a number of biomarkers, such as H_2O_2, L-cysteine, glucose, dopamine, glutathione, nucleic acids, proteins, and even cells.[2,3] However, the further applications of enzyme-based biosensors are limited by their high cost, instability in the nonphysiological environments, and difficulty in storage. In this circumstance, abundant nanomaterials with enzyme-like activities have been developed as substitutes for natural enzymes for detecting biomarkers due to their low cost, high stability, broad working temperature and pH, easy storage, and tunable sensing activity and selectivity.[4–6]

To date, more than fifty types of nanomaterials have been found with diverse enzyme-like activities (peroxidases (PODs), oxidases (OXDs), glucose oxidases (GOxs), and so on),[7–9] such as the noble metals,[10–12] metal oxides,[13–15] carbon nanostructures,[16–20] and metal–organic frameworks (MOFs).[21–24] However, the high cost of noble metals, the low operational stability and high cytotoxicity of metal oxides, the poor accuracy of carbon-based materials due to their high absorbabilities to substrates, severally hindering their applications as sensors for detecting biomarkers. To meet the ever-increasing demands of sensors in biological applications, it is still urgent to explore new nanomaterials with satisfied detecting activity and physicochemical properties.

Polymeric materials have been gradually recognized as potential candidates to meet the above requirements on designing next-generation biosensors.[25,26] However, owing to their low electron transferability, unsatisfactory enzyme-like activity, and poor sensing stability, it is still challenging to construct polymeric material-based biosensors with high sensitivity when compared with the state-of-the-art enzyme-like nanomaterial-based biosensors. Recent studies revealed that the phthalocyanine-based polymeric materials display unique advantages over traditional polymers, such as a strong π

[a] F. Chen, H. Zhu, N. Lv, Q. Li, Prof. X. Luo, Prof. C. Cheng
College of Polymer Science and Engineering
State Key Laboratory of Polymer Materials Engineering
Sichuan University
Chengdu 610065 (China)
E-mail: luoxl_scu@126.com

[b] Dr. T. Ma, Dr. L. Wang, Dr. S. Cao
Department of Ultrasound, West China Hospital
Sichuan University
Chengdu 610041 (China)
E-mail: caosujiao@scu.edu.cn

[c] Dr. M. Zhou
College of Biomass Science and Engineering
Sichuan University
Chengdu 610065 (China)

Supporting information for this article is available on the WWW under https://doi.org/10.1002/chem.202104591

conjugated system, high π-d delocalization effect of electrons, good conductivity, excellent metal-chelating property, and high chemical stability, which may eventually lead to high enzyme-like sensing activity.[27,28]

Here, in this study, we report a new colorimetric sensor based on copper phthalocyanine conjugated polymer nanoparticles, named as Cu-PcCP NPs, for detecting various biomarkers. A microwave-assisted polymerization is utilized to prepare the Cu-PcCP NPs, and their chemical structures are systematically explored. The colorimetric results of Cu-PcCP NPs demonstrate not only excellent enzyme-like detecting sensitivity but also great substrate selectivity than most of the reported Cu-based nanomaterials. In detail, the Cu-PcCP NPs can achieve a detection limit of 4.88 μM for the H_2O_2, 4.27 μM for the L-cysteine, and 21.10 μM for the glucose via a cascade catalytic system, which were comparable to many earlier reported enzyme-like nanomaterials. Moreover, the Cu-PcCP NPs present noticeable stability and remarkable resistance to harsh conditions, such as high temperatures and low pH, overcoming the current limitations of polymeric material-based biosensors and offering a new direction for designing next-generation enzyme-like nanomaterial-based colorimetric sensors.

Results and Discussion

Synthesis and Characterization

The Cu-PcCP NPs were synthesized via a facile microwave-assisted polymerization of a benzene-1,2,4,5-tetracarbonitrile building block with $CuCl_2$, where the addition of 1,8-Diazabicyclo[5.4.0]undec-7-ene (DBU) guaranteed the formation of conjugated networks through cyclization (Figure 1a, Figure S1).[29] The scanning electron microscopy (SEM) (Figure 1b, Figure S2) and transmission electron microscopy (TEM) (Figure 1c) show that the Cu-PcCP NPs present a spherical morphology of about 200 nm while the control sample, phthalocyanine-based conjugated polymer (PcCP) without Cu, presents a 2D-like microscale morphology (Figure S3). The morphologic difference indicates that the Cu ions play an essential role in regulating the spherical morphology. The crystalline structure and elemental distribution are analyzed by high-angle annular dark-field scanning transmission electron microscopy (HAADF-STEM). Figure 1d and Figure S4 show that there is no obvious crystal structure observed for Cu-PcCP NPs. The amorphous morphology is further confirmed by the obtained selected area electron diffraction (SAED, Figure 1e), which displays no apparent bright spots. The powder X-ray diffraction (PXRD) patterns (Figure 1f) only give a typical conjugated polymer peak at about 26° of Cu-PcCP NPs, and no crystalline peaks of Cu (JCPDS no. 04-0836) or CuO (JCPDS no. 34–1354) appear, which are consistent with the STEM and SAED data. The energy dispersive spectroscopy (EDS) patterns (Figure 1g) confirm the existence of Cu in the conjugated phthalocyanine-based polymers, and elemental mapping (Figure 1h) shows the homogeneous distribution of C, N, Cu atoms. Figure 1i,j present the EDS line scanning elemental signals, and there are relatively low but uniform Cu and N signals along the whole plane of materials, indicating the formation of Cu–N coordination structures.

Then, the chemical structures were thoroughly investigated. First, the ^{13}C NMR spectrum displays three peaks at 165.5, 133.4, and 115.9 ppm, which attribute to the phthalocyanine macrocycle in the phthalocyanine-based conjugated polymer network (Figure S5). The Raman spectra are used to study the carbon structure of Cu-PcCP NPs (Figure 2a) and the in-plane vibrations of the phthalocyanine molecule are verified as shown in A_{1g}, B_{1g}, and B_{2g} modes at 677, 744, and 1456 cm^{-1}, respectively.[30] Moreover, Fourier transform infrared (FTIR) spectroscopy (Figure 2b) reveals that the signal at 1118 cm^{-1} decreases dramatically compared to the copper phthalocyanine (CuPc) small molecules, indicating decreased peripheral C–H in-plane bending vibration on the benzene ring and confirming the polymerization of phthalocyanine monomers into the Cu-PcCP NPs.[28] Most importantly, ultraviolet-visible (UV-vis) spectra are applied to detect the conjugated structure, and the distinct blue shifts of B band and redshifts of Q bands for Cu-PcCP NPs (compared with CuPc motif) are observed (Figure 2c), which demonstrates the generation of the extended conjugated structure by linking benzene ring.[31]

The detailed valence state and atom ratio of Cu coordinated structure are further probed by X-ray photoelectron spectroscopy (XPS). As shown in Figure S6, the existence and atom ratio of C (69.2 at%), N (11.0 at%), and Cu (1.1 at%) in Cu-PcCP NPs are confirmed. Meanwhile, the high-resolution XPS spectrum of Cu 2*p* orbital clearly verifies the simultaneous presence of Cu (I) and Cu (II) (Figure 2d), in which Cu (I) is dominant (63.75 %). Additionally, the N 1s spectrum of Cu-PcCP NPs (Figure 2e) displays not only the isoindole rings (–N_β=, 400.19 eV), but also the nitrogen atoms adjacent to the central Cu (–N–M, 398.86 eV), suggesting the good coordination between phthalocyanine ring cavities with Cu ions. As demonstrated in Figure 2f, it could be deconvoluted into C_α, C_β, C_γ, and π-π* satellite peaks in the case of C 1s spectrum. The high intensity of the deconvoluted π-π* in relation to the Cu-PcCP NPs can be ascribed to the extended conjugation and strong bonding between the central Cu ions and phthalocyanine macrocycles.[32] The above data confirm the successful construction of the Cu-coordinated phthalocyanine polymeric skeleton. For the control sample, PcCP, the corresponding FTIR spectra, and XPS survey spectra also confirm the successful synthesis of metal-free phthalocyanine polymers (Figure S7).

Enzyme-like Sensing Activity

After validating that the Cu-PcCP NPs display a well Cu-coordinated phthalocyanine-based conjugated network, which shares a similar structure to the metal-N_4 catalytic active structure of many PODs, such as horseradish peroxidase (HRP), it is supposed that the Cu-PcCP NPs can be acted as a novel enzyme-like nanoplatforms for detecting biomarkers. Therefore, in the following sections, we will carefully study the detection sensitivity, selectivity, and stability of the Cu-PcCP NPs.

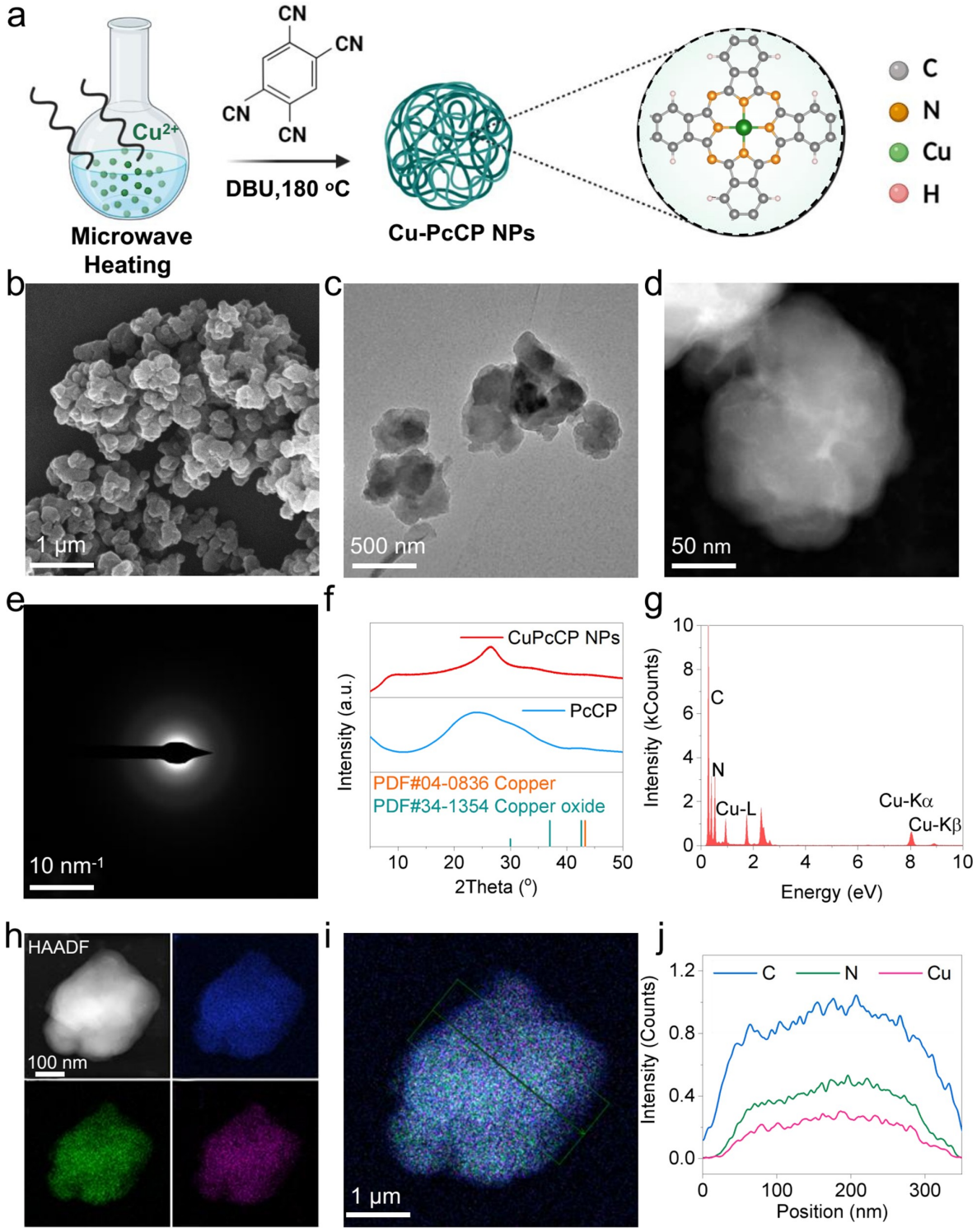

Figure 1. Fabrication of Cu-PcCP NPs and their morphological characterizations. (a) Schematic illustration of the synthetic route, (b) SEM, (c) TEM, (d) HAADF-STEM image, (e) SAED pattern of Cu-PcCP NPs. (f) Typical PXRD patterns of Cu-PcCP NPs and PcCP. (g) Corresponding EDS pattern of Cu-PcCP NPs. (h) HAADF-STEM elemental mapping of C (blue), N (green), Cu (pink), and (i) elements merge. (j) EDS line scan signal of Cu-PcCP NPs in (i).

As a typical chromophoric substrate, 3,3′,5,5′-tetramethylbenzidine (TMB) is often utilized for examining the enzyme-like activity.[33] The essay demonstrates that Cu-PcCP NPs can rapidly catalyze the oxidation of TMB (transparent) by decomposing H_2O_2 to produce oxTMB (blue color) with a great increasing characteristic absorbance at 652 nm, while the PcCP and CuPc show negligible enzyme-like activities (Figure 3a,b). This is mainly owing to the π-conjugated structure of Cu-PcCP

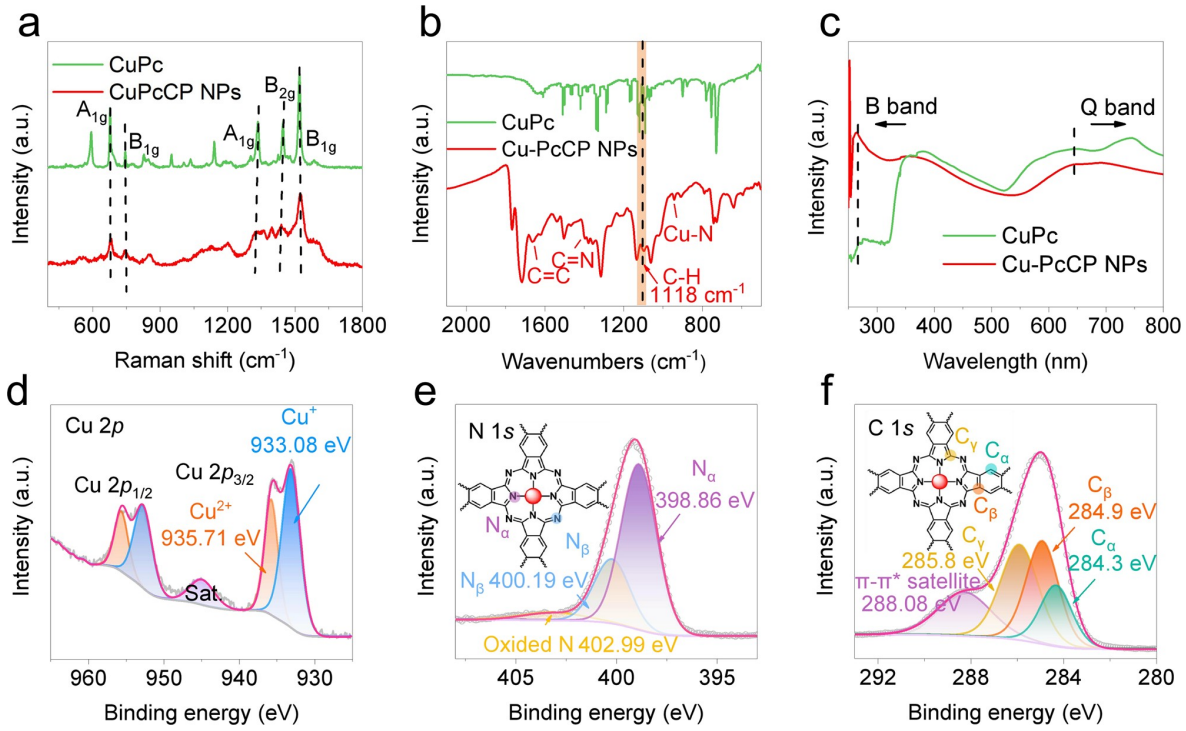

Figure 2. The structural characterization of Cu-PcCP NPs. (a) Raman, (b) FTIR, (c) UV-vis spectra of Cu-PcCP NPs and commercial CuPc. High-resolution XPS spectra for Cu 2*p* (d), N 1s (e) and C 1s (f) of Cu-PcCP NPs.

NPs that facilitating hydrogen atoms transfer from the amino group of TMB to the hydroxyl adsorbate.[34] As expected, the POD-like activity relies on the concentrations of Cu-PcCP NPs and displays a time-dependent manner (Figure 3c,d). When Cu-PcCP NPs are used in harsh conditions, they maintain a high enzyme-like activity over a wide range of pH conditions and temperatures (Figure 3e,f), which are much superior to natural enzymes (e. g., HRP).[35] We repeatedly conducted the POD-like activity test via a TMB colorimetric method to verify the cyclic catalytic ability. The results show that there is no apparent loss of catalytic activity during the test, indicating good catalytic stability of the Cu-PcCP NPs (Figure S8a). Besides, the Cu-PcCP NPs also show excellent stability in the acetic acid-sodium acetate buffer (pH 4.5), and the catalytic performance maintains well even after soaking for 30 days (Figure S8b).

The steady-state kinetic assay is performed to examine the POD-like activity of Cu-PcCP NPs. By using H_2O_2 and TMB as the substrate, the enzyme kinetic constants (K_m, V_{max}, K_{cat}, and K_{cat}/K_m) of Cu-PcCP NPs are determined. The typical Michaelis-Menten kinetic curves are acquired from Cu-PcCP NPs-triggered catalytic reactions (Figure 4a,c), and their Lineweaver-Burk double reciprocal plots reflect a good linear relationship with H_2O_2 and TMB, respectively (Figure 4b,d). Compared with the reported works, the lower K_m and higher V_{max} values of Cu-PcCP NPs indicate that they have stronger substrate affinity and faster reaction velocity than most Cu-based nanomaterials. What's more, the K_{cat} and K_{cat}/K_m are also important parameters to measure the catalytic efficiency (Table 1), which can verify the outstanding catalytic performance of Cu-PcCP NPs. It is noteworthy that Cu-PcCP NPs also display excellent enzyme-like activity and advantages over other Cu-based and many earlier reported transition metal-based nanomaterials (Figure 4e, Table S1), further illustrating the extraordinary catalytic performance of Cu-PcCP NPs.

In order to gain insights into the enzyme-like catalytic mechanism of Cu-PcCP NPs, we conducted electron paramagnetic resonance (EPR) to detect the intermediate reactive oxygen species (ROS) by applying 5,5-Dimethyl-1-pyrroline N-oxide (DMPO) as the spin trapping agent.[41] As shown in Figure 5a, the characteristic peak of the DMPO/$^{\bullet}$OH adducts exhibit a clear signal intensity of 1:2:2:1, implying that Cu-PcCP NPs have generated $^{\bullet}$OH during the decomposition of H_2O_2. Terephthalate (TA) is chosen as a fluorescent probe to further detect the $^{\bullet}$OH (Figure 5b). The fluorescence intensity (at 440 nm) of the reaction solution increases slightly after adding Cu-PcCP NPs, also confirming the production of $^{\bullet}$OH. Moreover, the EPR analysis has a signal intensity of 1:1:1:1:1:1 when the reaction solution is replaced by dimethyl sulfoxide (a scavenger for $^{\bullet}$OH) (Figure 5c), indicating that Cu-PcCP NPs can produce $O_2^{\bullet-}$ during the decomposition of H_2O_2. And the $O_2^{\bullet-}$ intermediate can also be captured via an $O_2^{\bullet-}$-specific probe hydroethidine (HE) (Figure 5d). However, the production of $^1O_2$ was not detected either from EPR or fluorescence experiments (Figure S9), so the free radicals involved in the test reaction are $^{\bullet}$OH and $O_2^{\bullet-}$.

In order to distinguish the relative generation amount of ROS, tertiary butanol (TBA) and p-benzoquinone (BQ) are utilized as scavengers for $^{\bullet}$OH and $O_2^{\bullet-}$, respectively. As shown

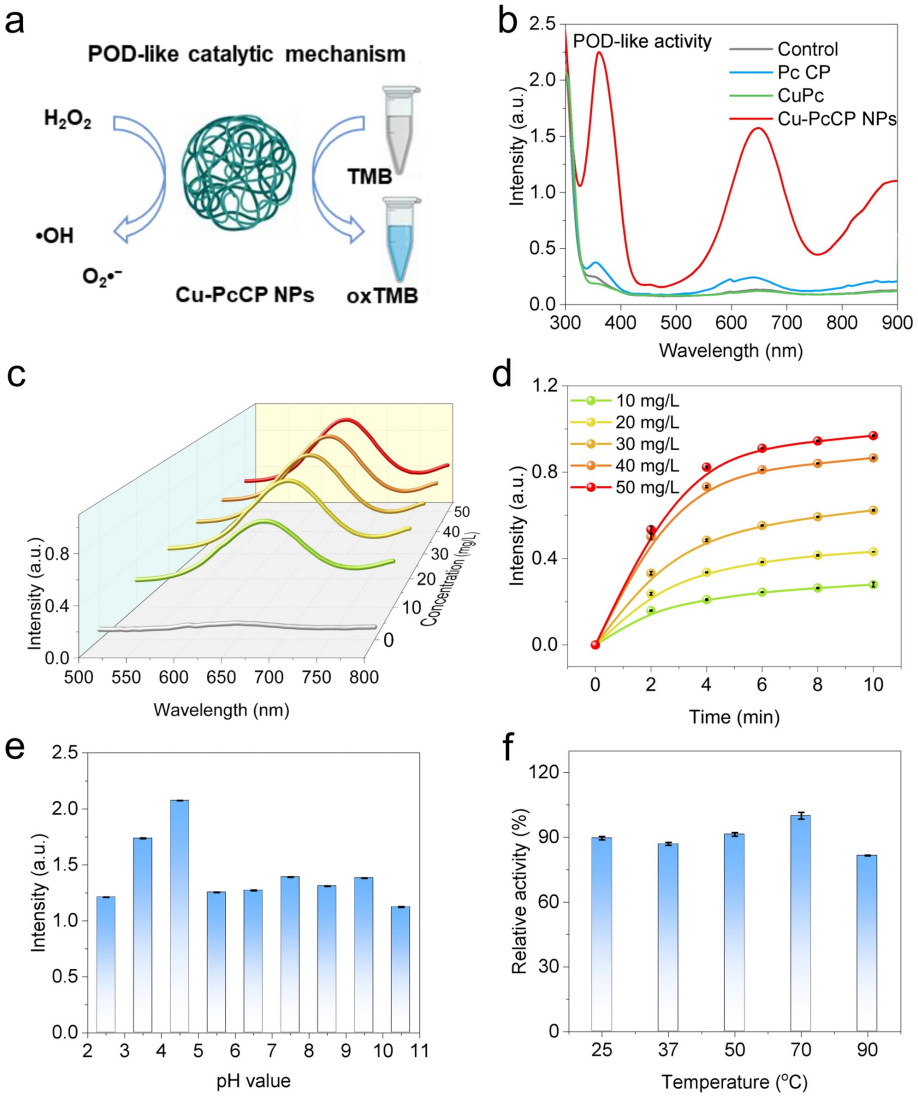

Figure 3. Enzyme-like performance of the Cu-PcCP NPs via using TMB as substrate. (a) Schematic illustration of POD-like catalytic mechanism of Cu-PcCP NPs. (b) UV-vis absorption spectra of the reaction solution containing with or without PcCP, CuPc, and Cu-PcCP NPs. (c) UV-vis absorption spectra of the reaction solution containing varying concentrations of Cu-PcCP NPs. (d) Time-dependent absorbance changes of oxTMB with varying concentrations of Cu-PcCP NPs. (e) and (f) POD-like activity of Cu-PcCP NPs under various pH conditions and temperatures, respectively, where the absorbance at pH 4.5 was defined as 100%. The error bars were calculated from three measurements.

Table 1. Catalytic performance comparison of this work with earlier reported Cu-based nanomaterials.

Enzyme-like nanomaterials	Substrate	K_m [mM]	V_{max} [10^{-8} M s^{-1}]	K_{cat} [10^{-3} s^{-1}]	K_{cat}/K_m [s^{-1} M^{-1}]	Ref.
Cu-PcCP NPs	H_2O_2	8.86	198.56	50.13	5.67	This work
	TMB	0.11	30.50	7.70	72.64	
CuO	H_2O_2	31.18	28.00	2.23	0.07	[36]
$Cu(OH)_2$	H_2O_2	28.91	34.00	3.33	0.12	[36]
CuNPs/N-C	H_2O_2	17.98	8.57	3.32	0.18	[37]
	TMB	1.57	12.80	4.95	3.15	
Cu nanozyme	H_2O_2	7.90	10.30	4.50	0.08	[38]
	TMB	0.25	21.50	7.30	12.60	
Cu_xO	H_2O_2	52.30	23.70	4.50	0.08	[39]
	TMB	0.58	38.40	7.30	12.60	
$CuFe_2O_4$	H_2O_2	0.50	2.61	2.09	4.18	[40]
	TMB	2.26	2.07	0.30	0.13	

K_m is the Michaelis constant, V_{max} is the maximal reaction velocity. K_{cat} is the catalytic constant. K_{cat}/K_m value indicates the catalytic efficiency.

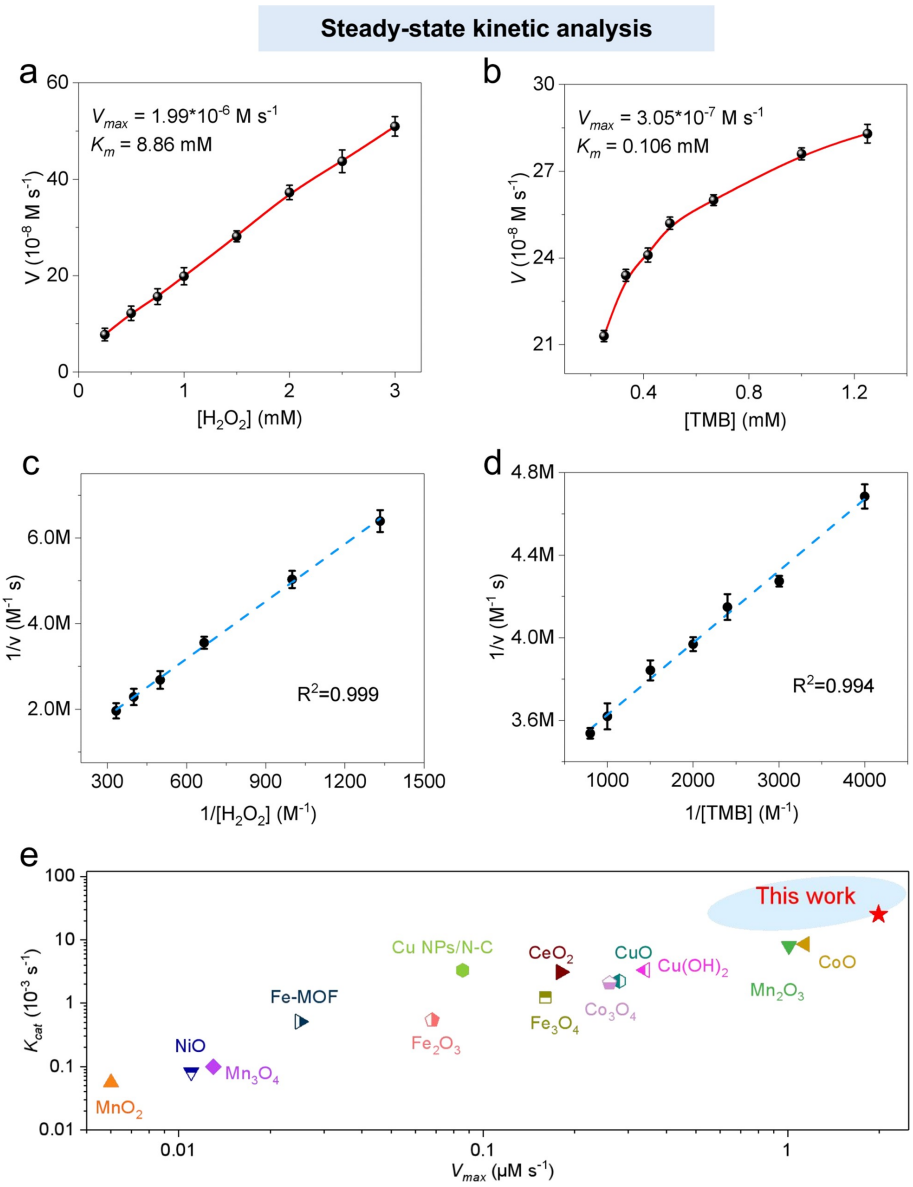

Figure 4. Steady-state kinetic analysis of the Cu-PcCP NPs. Michaelis-Menten curves for (a) H_2O_2 and (b) TMB. The error bars were obtained by three measurements. Lineweaver-Burk plot for (c) H_2O_2 and (d) TMB. (e) Catalytic performance comparison of this work with earlier reported transition metal-based nanomaterials.

in Figure S10, the absorbance of oxTMB decreases rapidly regardless of adding TBA or BQ, showing that the $^{\bullet}OH$ and $O_2^{\bullet-}$ intermediates both play important roles in the POD-like activity of Cu-PcCP NPs. Meanwhile, the BQ has a greater impact on the absorbance, which certifies that the POD-like activity of Cu-PcCP NPs is mainly attributed to the production of $O_2^{\bullet-}$ during the decomposition of H_2O_2.

Colorimetric Detection of H_2O_2

Since H_2O_2 plays a critical role in the living system, the quantitative detection of H_2O_2 concentration possesses great significance in biosensing application fields. As shown in Figure 6a, the absorbance at 652 nm increases gradually with elevated H_2O_2 concentrations in the presence of Cu-PcCP NPs. By analyzing the linear calibration diagram in the range of 5–100 μM (Figure 6b), the correlation coefficient was found to be 0.99817. Meanwhile, the calculated limit of detection (LOD) for H_2O_2 is 4.88 mM. The relative standard deviation (RSD) for LOD was 1.1 % (n = 3). As shown from Table S2, Cu-PcCP NPs have a relatively lower LOD and wider range than other nanomaterials, thus proving that the Cu-PcCP NPs can act as an ideal biosensor for H_2O_2, which lays the foundation for further cascade detection.

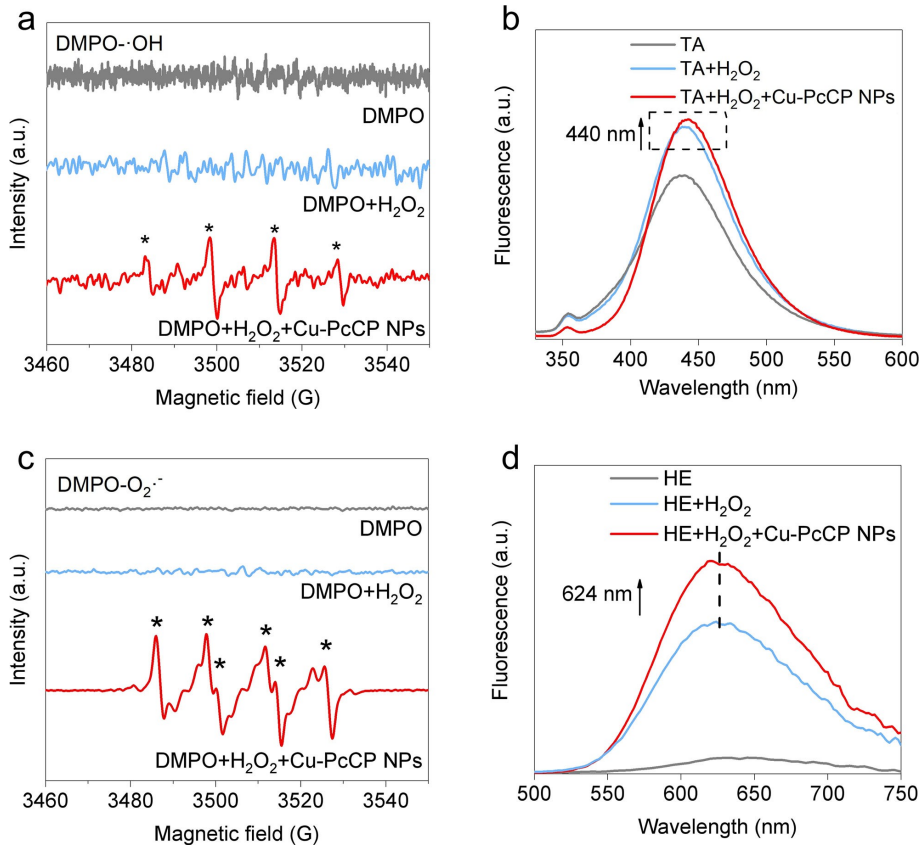

Figure 5. Investigations of enzyme-like catalytic process and radical species. (a) EPR spectra of the spin adduct of the DMPO/•OH generated during the decomposition of H_2O_2. (b) Detection of •OH by applying TA as the fluorescent probe. (c) EPR spectra of the spin adduct of the DMPO/$O_2^{\bullet-}$ generated during the decomposition of H_2O_2. (d) Detection of $O_2^{\bullet-}$ by using HE as a fluorescent probe.

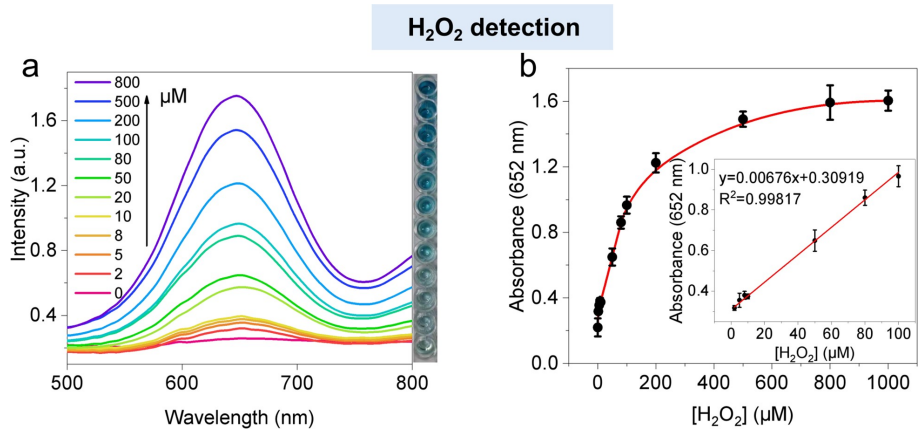

Figure 6. Colorimetric detection of H_2O_2 by the Cu-PcCP NPs. (a) UV-vis absorption spectra of the reaction solution with varying concentrations of H_2O_2. (b) Dose-response curve for H_2O_2 detection. Inset: linear calibration plot for H_2O_2. The error bars represent the standard deviation obtained from three parallel experiments.

Colorimetric Detection of L-cysteine

L-cysteine, a typical semi-essential amino acid for human beings, plays a vital role in various cell functions, such as protein synthesis, metabolism, and detoxification.[42] Thus, establishing a quantitative method to detect L-cysteine rapidly is worth considering.[43] It has been reported that L-cysteine can inhibit the enzyme-like activity of nanomaterials through the interaction of –SH with metal active centers, thus resulting in changes of oxTMB absorbance.[44] Based on this unique mechanism, diverse metal-based POD-like nanomaterials have been designed to detect L-cysteine.[44,45] Due to the excellent

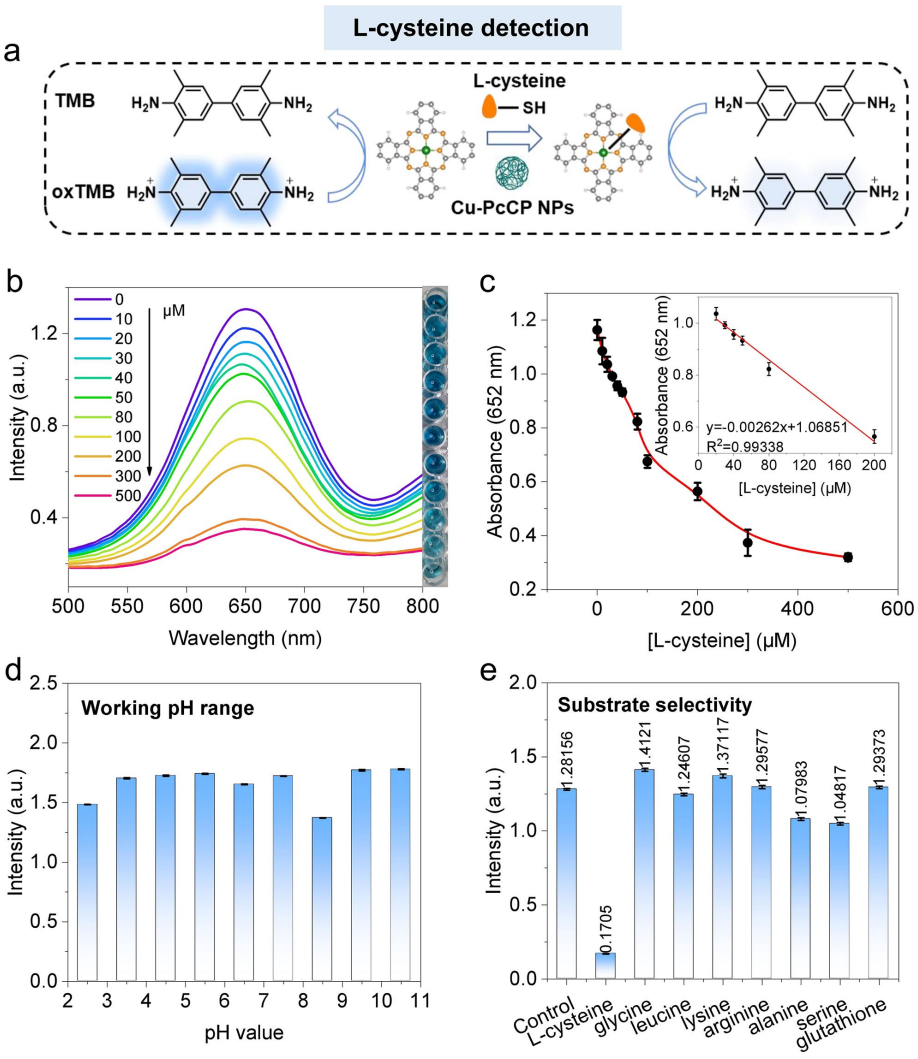

Figure 7. Colorimetric detection of L-cysteine by the Cu-PcCP NPs. (a) Schematic illustration of the detecting mechanism. (b) UV-vis absorption spectra of the reaction solutions in the presence of various concentrations of L-cysteine. (c) Dose-response inhibition curve for L-cysteine detection. Inset: linear calibration plot for L-cysteine. (d) Influence of working pH on the detecting performance. (e) Selectivity analysis by detecting the absorbance in the presence of L-cysteine or the interferences. The error bars represent the standard deviation of three measurements.

POD-like activity of Cu-PcCP NPs, the catalytic sensing of L-cysteine is carefully investigated via TMB mediated POD-like activity assay (Figure 7a). As shown in Figure 7b, the absorbance of oxTMB decreases gradually with the increase of L-cysteine concentration, presenting a dose-response inhibition manner. The linear calibration curve ranges from 20 to 200 μM (R^2 = 0.99338), and the calculated LOD is about 4.27 μM (n = 3) (Figure 7c). Although the LOD of Cu-PcCP NPs is slightly higher than that of other nanomaterials, notably, the detection range and concentration of L-cysteine are obviously larger (Table 2). Additionally, we find that the Cu-PcCP NPs can maintain a good detection ability for L-cysteine in a wide range of pH conditions (Figure 7d). The selectivity of L-cysteine detection was also verified by several amino acids, homocysteine, and glutathione as interfering substances (Figure 7e). The results show that the Cu-PcCP NPs-based sensing system is resistant to other interferences and has good selectivity for L-cysteine. However, the distinction between L-cysteine and homocysteine remains highly challenging due to their high structural similarity. In view of the high sensitivity, selectivity, and stability of Cu-PcCP NPs, their applicability for detecting L-cysteine in human serum was studied. According to the results displayed in Table S3, the recovery rates of L-cysteine range from 98.1 to 103.4%, and the

Table 2. Performance comparison of Cu-PcCP NPs with other reported metal-based nanomaterials in detecting L-cysteine.

Enzyme-like nanomaterials	Linear range [μM]	LOD [μM]	Ref.
Cu-PcCP NPs	20–200	4.27	This work
$Ga(OH)_3$	0.2–75	2.60	[44]
Cu_2O NPs	0–10	0.81	[46]
MoS_2-PPy-Pd	1–10	0.08	[47]
MoS_2-Au@Pt	0.8–54.4	0.50	[48]
CeO_2/CoO NCs	5–10	3.71	[49]
CuO/ZnO nanocomposites	40–96	40.00	[50]

RSD is limited to 1.2–2.7%, proving the potential of Cu-PcCP NPs in clinical diagnosis.

Colorimetric Detection of Glucose

The blood glucose level is an essential physiological parameter, and an excessive amount will lead to many endocrine-based metabolic diseases.[51] Therefore, it is essential to develop a sensitive, low-cost, and simple glucose biosensor. Combining the cascade catalytic activity of GOx (decomposition of glucose into H_2O_2) with the POD-like activity of Cu-PcCP NPs, we designed a biosensing platform integrated with GOx and Cu-PcCP NPs to detect glucose concentration (Figure 8a). As shown in Figure 8b, with the increase of glucose concentration, the absorbance at 652 nm gradually rises, thus proving the high sensitivity of the method for glucose detection. As can be seen from the dose-responsive curve (Figure 8c), the calculated linear calibration curve of the glucose ranges from 0 to 600 μM, with LOD as low as 21.1 μM (n = 3). It is noteworthy that the glucose sensor constructed by GOx and Cu-PcCP NPs has a comparable detection limit and even a wider linear range when compared with many other glucose sensors, as summarized in Table 3. Meanwhile, this hybrid sensor can maintain a good detection ability for glucose under a wide range of pH conditions (Figure 8d). Furthermore, the interfering substances, for instance, glucose analogs, ions, and glutathione, have been utilized to disclose the interference resistance of Cu-PcCP NPs (Figure 8e), and the results show that the detection system has very good selectivity for glucose. In order to study the interference of O_2 in the cascade catalytic system, which may be decomposed by OXD-like nanomaterials and subsequently oxidize the TMB, the OXD-like enzyme activity of Cu-PcCP NPs is also evaluated. Interestingly, Cu-PcCP NPs exhibit negligible OXD-like activity, thus avoiding the interference of O_2 in the detection process (Figure S11). Moreover, to verify the feasibility

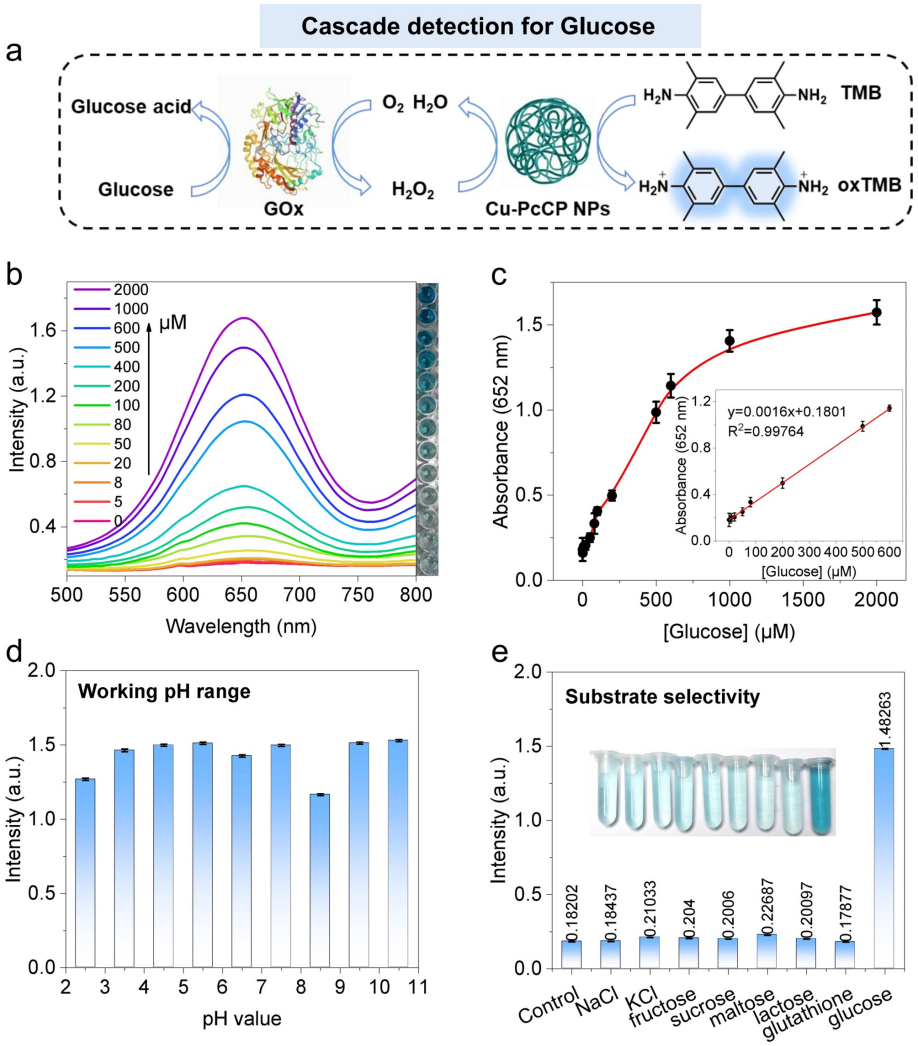

Figure 8. Cascade colorimetric detection of glucose by the Cu-PcCP NPs. (a) Schematic illustration of the proposed cascade detection biosensor. (b) UV-vis absorption spectra of the reaction solution containing varying concentrations of glucose. (c) Dose-response curve for glucose detection. Inset: linear calibration plot for glucose. (d) Influence of working pH on the detecting performance. (e) Selectivity analysis by detecting the absorbance in the presence of glucose or interferences. The error bars represent the standard deviation of three measurements.

Table 3. Performance comparison of the Cu-PcCP NPs with earlier reported nanomaterials in glucose detection.

Enzyme-like nanomaterials	Linear range (μM)	LOD [μM]	Ref.
Cu-PcCP NPs	0–600	21.1	This work
CuNiAl LDH	10–200	2.9	[52]
Zn-CuO	25–500	1.5	[53]
CuBDC	10–500	4.1	[54]
TiO_2-CeO_2	10–500	6.1	[55]
GO_x-hemin nanogels	0–256	4.0	[56]
Au@Pt nanorods	45–400	45.0	[57]
$CoPW_{11}O_{39}$	33–500	23.4	[58]

of Cu-PcCP NPs in practical application, the standard addition method was performed to determine glucose concentration in the human serum. As listed in Table 4, the recovery rates of glucose range from 97.9% to 98.2% with RSD limited to 1.4-2.6%. Therefore, the developed cascade detection biosensor presents high sensitivity, selectivity, stability in glucose sensing, which may have a broad application prospect in biological analysis and medical diagnosis. At last, the potential cellular toxicity of Cu-PcCP NPs was verified using the CCK-8 assay. The HUVEC cells can maintain considerable viability after co-cultured with Cu-PcCP NPs even at a high concentration (12.5 μg/mL), indicating the good cell compatibility of Cu-PcCP NPs (Figure S12) and their promising potential for the detection of biomolecules in cellular condition.

Conclusion

In summary, we have successfully developed a new type of biosensor for detecting various biomarkers. Through microwave-assisted polymerization, the as-prepared Cu-PcCP NPs feature strong metal-chelation, fast electron transfer, and good chemical stability, which are suitable for the construction of biosensors. Impressively, the Cu-PcCP NPs display excellent enzyme-like detecting sensitivity and remarkable substrate selectivity than most of the reported Cu-based nanomaterials. And the Cu-PcCP NPs exhibit appealing performance for sensitively detection of H_2O_2, L-cysteine, and glucose with LODs of 4.88, 4.27, and 21.10 μM, respectively. Moreover, the Cu-PcCP NPs show excellent catalytic stability in different pH and temperature conditions, which effectively overcome the current limitations of many polymeric material-based sensors. Thus, we believe that this work offers a promising strategy for the rational design of next-generation enzyme-like nanomaterials to detect various biomarkers.

Supporting Information

Supplementary data are available from the Supporting Information, including materials; materials characterization; synthesis of Cu-PcCP NPs; enzyme-like sensing activity; steady-state kinetic study; active intermediates identification; colorimetric sensing of H_2O_2, L-cysteine and glucose; SEM image; HAADF-STEM; XRD patterns; XPS survey scanning; N 1s XPS spectra; FTIR spectra; solution stability of Cu-PcCP NPs; OXD-like activity; effects of scavengers on the enzyme-like activity of Cu-PcCP NPs; table for comparison of POD-like activity and H_2O_2 detection ability of Cu-PcCP NPs with recently reported nanomaterials; recovery tests for L-cysteine analysis in human serum.

Author Contributions

F.C. conceived the idea and designed the project. F.C. performed the major experiments and analyzed the results. H.Z., T.M., L.Y.W., M.Z., N.L., and Q.L. assisted with the data analysis and figure production. F.C., S.J.Cao., X.L.L., and C.C. wrote and edited the manuscript. S.J.Cao., X.L.L., and C.C. supervised the whole project. All authors discussed the results and commented on the manuscript.

Acknowledgements

This work was financially supported by the National Key R&D Program of China (2019YFA0110600 and 2019YFA0110601), National Natural Science Foundation of China (Nos. 51973130, 52161145402, 52173133, 51903178, 82102065), the Science and Technology Project of Sichuan Province (Nos. 2021YFH0087, 21YYJC2714, 2021YFH0135, 2021YJ0434, 2021YJ0554), China Postdoctoral Science Foundation (2021M692303, 2021M702334), the 1·3·5 Project for Disciplines of Excellence, West China Hospital, Sichuan University (No. ZYJC21047), and Full-time Postdoctoral Foundation of Sichuan University (2021SCU12013), Post-Doctor Research Project, West China Hospital, Sichuan University (2020HXBH126). Prof. Cheng acknowledges the financial support of the State Key Laboratory of Polymer Materials Engineering (Grant No. sklpme2021-4-02). The authors thank the Ceshigo and Zhongkebaice Technology Service Co., Ltd. for the technical support of XPS and TEM. We gratefully acknowledge Dr. Chao He and Dr. Minghua Zhang for their analytical support.

Table 4. Recovery tests for glucose analysis in human serum using the proposed assay (n = 5).

Sample	Measured before [μM]	Added glucose [μM]	Measured after [μM]	Recovery [%]	RSD [%]
1	430.3	70	490.8	98.1%	1.4%
2	431.6	100	520.2	97.9%	1.3%
3	428.4	150	567.9	98.2%	2.6%

Conflict of Interest

The authors declare no conflict of interest.

Data Availability Statement

The data that support the findings of this study are available from the corresponding author upon reasonable request.

Keywords: biosensor · colorimetric detection · conjugated polymer · copper phthalocyanine · enzyme-like nanomaterials

[1] S. Song, Y. Qin, Y. He, Q. Huang, C. Fan, H.-Y. Chen, *Chem. Soc. Rev.* **2010**, *39*, 4234–4243.
[2] J. I. Reyes-De-Corcuera, H. E. Olstad, R. García-Torres, *Annu. Rev. Food Sci. Technol.* **2018**, *9*, 293–322.
[3] C. Chen, Z. Wu, P. Ding, N. Sun, H. Liu, Y. Chen, Z. Wang, R. Pei, *Adv. Fiber Mater.* **2020**, *2*, 186–193.
[4] J. Wu, X. Wang, Q. Wang, Z. Lou, S. Li, Y. Zhu, L. Qin, H. Wei, *Chem. Soc. Rev.* **2019**, *48*, 1004–1076.
[5] M. Liang, X. Yan, *Acc. Chem. Res.* **2019**, *52*, 2190–2200.
[6] Y. Huang, J. Ren, X. Qu, *Chem. Rev.* **2019**, *119*, 4357–4412.
[7] H. Dong, Y. Fan, W. Zhang, N. Gu, Y. Zhang, *Bioconjugate Chem.* **2019**, *30*, 1273–1296.
[8] L. Li, L. J. Cao, X. Xiang, X. Z. Wu, L. Ma, F. Chen, S. J. Cao, C. Cheng, D. W. Deng, L. Qiu, *Adv. Funct. Mater.* **2021**, 2107530.
[9] H. Liu, Y. You, Y. Sang, F. Pu, J. Ren, X. Qu, *Chem. Eur. J.* **2021**, *27*, 18201–18207.
[10] G. Fang, W. Li, X. Shen, J. M. Perez-Aguilar, Y. Chong, X. Gao, Z. Chai, C. Chen, C. Ge, R. Zhou, *Nat. Commun.* **2018**, *9*, 129.
[11] G.-J. Cao, X. Jiang, H. Zhang, T. R. Croley, J.-J. Yin, *RSC Adv.* **2017**, *7*, 52210–52217.
[12] S. He, L. Yang, P. Balasubramanian, S. Li, H. Peng, Y. Kuang, H. Deng, W. Chen, *J. Mater. Chem. A* **2020**, *8*, 25226–25234.
[13] Q. Liu, A. Zhang, R. Wang, Q. Zhang, D. Cui, *Nano-Micro Lett.* **2021**, *13*, 154.
[14] J. Wu, Q. Yang, Q. Li, H. Li, F. Li, *Anal. Chem.* **2021**, *93*, 4084–4091.
[15] J. Wu, W. Lv, Q. Yang, H. Li, F. Li, *Biosens. Bioelectron.* **2021**, *171*, 112707.
[16] X. Wang, H. Wang, S. Zhou, *J. Phys. Chem. Lett.* **2021**, *12*, 11751–11760.
[17] M. C. A. de Oliveira, E. G. de L. Oliveira, I. C. B. Pires, I. C. M. Candido, N. Rakov, H. P. de Oliveira, Y. Xing, G. S. Maciel, *Adv. Fiber Mater.* **2020**, *2*, 302–313.
[18] Y. Wang, N. Zhang, R. Hübner, D. Tan, M. Löffler, S. Facsko, E. Zhang, Y. Ge, Z. Qi, C. Wu, *Adv. Mater. Interfaces* **2019**, *6*, 1801664.
[19] Y. Long, L. Li, T. Xu, X. Wu, Y. Gao, J. Huang, C. He, T. Ma, L. Ma, C. Cheng, C. Zhao, *Nat. Commun.* **2021**, *12*, 6143.
[20] W. Lv, X. Wang, J. Wu, H. Li, F. Li, *Chin. Chem. Lett.* **2019**, *30*, 1635–1638.
[21] L. Ma, F. Jiang, X. Fan, L. Wang, C. He, M. Zhou, S. Li, H. Luo, C. Cheng, L. Qiu, *Adv. Mater.* **2020**, *32*, 2003065.
[22] Y. Wang, N. Zhang, D. Tan, Z. Qi, C. Wu, *Front. Bioeng. Biotechnol.* **2020**, *8*, 714.
[23] H. Chen, X. Li, M. Huo, L. Wang, Y. Chen, W. Chen, B. Wang, *Nano Res.* **2021**, *14*, 205–211.
[24] X. Liu, X. Gao, L. Yang, Y. Zhao, F. Li, *Anal. Chem.* **2021**, *93*, 11792–11799.
[25] D. Zhu, M. Zhang, L. Pu, P. Gai, F. Li, *Small* **2021**, e2104993.
[26] M. Yin, Z. Duan, C. Zhang, L. Feng, Y. Wan, Y. Cai, H. Liu, S. Li, H. Wang, *Microchem. J.* **2019**, *145*, 864–871.
[27] H. Zhong, M. Ghorbani-Asl, K. H. Ly, J. Zhang, J. Ge, M. Wang, Z. Liao, D. Makarov, E. Zschech, E. Brunner, I. M. Weidinger, J. Zhang, A. V. Krasheninnikov, S. Kaskel, R. Dong, X. Feng, *Nat. Commun.* **2020**, *11*, 1409.
[28] S. Yang, Y. Yu, M. Dou, Z. Zhang, L. Dai, F. Wang, *Angew. Chem. Int. Ed.* **2019**, *58*, 14724–14730; *Angew. Chem.* **2019**, *131*, 14866–14872.
[29] T. Haruhiko, S. Shojiro, S. Shinsaku, *Chem. Lett.* **1983**, *12*, 313–316.
[30] J. Chen, K. Zou, P. Ding, J. Deng, C. Zha, Y. Hu, X. Zhao, J. Wu, J. Fan, Y. Li, *Adv. Mater.* **2019**, *31*, e1805484.
[31] X. Ding, J. Guo, X. Feng, Y. Honsho, J. Guo, S. Seki, P. Maitarad, A. Saeki, S. Nagase, D. Jiang, *Angew. Chem. Int. Ed.* **2011**, *50*, 1289–1293; *Angew. Chem.* **2011**, *123*, 1325–1329.
[32] H. Wu, Y. Cao, G. Zhu, D. Zeng, X. Zhu, J. Du, L. He, *Chem. Commun.* **2020**, *56*, 3637–3640.
[33] B. Jiang, D. Duan, L. Gao, M. Zhou, K. Fan, Y. Tang, J. Xi, Y. Bi, Z. Tong, G. F. Gao, N. Xie, A. Tang, G. Nie, M. Liang, X. Yan, *Nat. Protoc.* **2018**, *13*, 1506–1520.
[34] X. Shen, Z. Wang, X. Gao, Y. Zhao, *ACS Catal.* **2020**, *10*, 12657–12665.
[35] L. Gao, J. Zhuang, L. Nie, J. Zhang, Y. Zhang, N. Gu, T. Wang, J. Feng, D. Yang, S. Perrett, X. Yan, *Nat. Nanotechnol.* **2007**, *2*, 577–583.
[36] X. Wang, X. J. Gao, L. Qin, C. Wang, L. Song, Y. N. Zhou, G. Zhu, W. Cao, S. Lin, L. Zhou, K. Wang, H. Zhang, Z. Jin, P. Wang, X. Gao, H. Wei, *Nat. Commun.* **2019**, *10*, 704.
[37] Y. Wu, J. Wu, L. Jiao, W. Xu, H. Wang, X. Wei, W. Gu, G. Ren, N. Zhang, Q. Zhang, L. Huang, L. Gu, C. Zhu, *Anal. Chem.* **2020**, *92*, 3373–3379.
[38] S. Naveen Prasad, P. Weerathunge, M. N. Karim, S. Anderson, S. Hashmi, P. D. Mariathomas, V. Bansal, R. Ramanathan, *Anal. Bioanal. Chem.* **2021**, *413*, 1279–1291.
[39] C. Hao, A. Qu, L. Xu, M. Sun, H. Zhang, C. Xu, H. Kuang, *J. Am. Chem. Soc.* **2019**, *141*, 1091–1099.
[40] F. Xia, Q. Shi, Z. Nan, *Dalton Trans.* **2020**, *49*, 12780–12792.
[41] Z. Wang, W. Ma, C. Chen, H. Ji, J. Zhao, *Chem. Eng. J.* **2011**, *170*, 353–362.
[42] K. G. Reddie, K. S. Carroll, *Curr. Opin. Chem. Biol.* **2008**, *12*, 746–754.
[43] S. Garcia-Santamarina, S. Boronat, E. Hidalgo, *Biochemistry* **2014**, *53*, 2560–2580.
[44] M. Singh, P. Weerathunge, P. D. Liyanage, E. Mayes, R. Ramanathan, V. Bansal, *Langmuir* **2017**, *33*, 10006–10015.
[45] P. D. Liyanage, P. Weerathunge, M. Singh, V. Bansal, R. Ramanathan, *Nanomaterials* **2021**, *11*, 1285.
[46] Y. Zhu, Z. Zhang, X. Song, Y. Bu, *J. Mater. Chem. B* **2021**, *9*, 3533–3543.
[47] M. Chi, Y. Zhu, L. Jing, C. Wang, X. Lu, *Anal. Chim. Acta* **2018**, *1035*, 146–153.
[48] L. Wan, L. Wu, S. Su, D. Zhu, J. Chao, L. Wang, *Chem. Commun.* **2020**, *56*, 12351–12354.
[49] J. Lian, P. Liu, C. Jin, Q.-Y. Liu, X. Zhang, X. Zhang, *ACS Sustainable Chem. Eng.* **2020**, *8*, 17540–17550.
[50] M. Šimšíková, J. Čechal, A. Zorkovská, M. Antalík, T. Šikola, *Colloids Surf. B* **2014**, *123*, 951–958.
[51] G. Danaei, M. M. Finucane, Y. Lu, G. M. Singh, M. J. Cowan, C. J. Paciorek, J. K. Lin, F. Farzadfar, Y.-H. Khang, G. A. Stevens, M. Rao, M. K. Ali, L. M. Riley, C. A. Robinson, M. Ezzati, *The Lancet* **2011**, *378*, 31–40.
[52] L. Wu, X. Zhou, G. Wan, Y. Tang, S. Shi, X. Xu, G. Wang, *Dalton Trans.* **2021**, *50*, 95–102.
[53] A. P. Nagvenkar, A. Gedanken, *ACS Appl. Mater. Interfaces* **2016**, *8*, 22301–22308.
[54] X. Cheng, Z. Zheng, X. Zhou, Q. Kuang, *ACS Sustainable Chem. Eng.* **2020**, *8*, 17783–17790.
[55] G. Vinothkumar, A. I. Lalitha, K. Suresh Babu, *Inorg. Chem.* **2019**, *58*, 349–358.
[56] X. Fan, J. Lim, Z. Li, T. Wang, L. Jiang, S. Liu, L. Zhou, C. He, *J. Mater. Chem. B* **2021**, *9*, 3509–3514.
[57] J. Liu, X. Hu, S. Hou, T. Wen, W. Liu, X. Zhu, J.-J. Yin, X. Wu, *Sens. Actuators B* **2012**, *166–167*, 708–714.
[58] Y. He, X. Li, X. Xu, J. Pan, X. Niu, *J. Mater. Chem. B* **2018**, *6*, 5750–5755.

Manuscript received: December 28, 2021
Accepted manuscript online: April 8, 2022
Version of record online: May 25, 2022